Journal of Heat and Mass Transfer Research 4 (2016) 83-90

Semnan University

Journal of Heat and Mass Transfer Research

Journal homepage: http://jhmtr.journals.semnan.ac.ir

Effect of baffle orientation on shell-and-tube heat exchanger performance

Ali Akbar Abbasian Arani, Ali Arefmanesh, Hamed Uosofvand*

Department of Mechanical Engineering, University of Kashan, Kashan, Iran

PAPER INFO

History:

Submitted 2016-09-01
Revised 2017-06-14
Accepted 2017-06-14

Keywords:

Shell-and-tube;
Heat exchanger;
Baffle;
Pressure drop;
Heat transfer

ABSTRACT

In this paper, fluid flow and heat transfer in a laboratory (i.e., small size) shell-and-tube heat exchanger are analyzed with computational fluid dynamic software. In this type of shell-and-tube heat exchanger, baffles with different angles of rotation (0° [horizontal segmental baffle], 15° [from horizontal], 30°, 45°, 60°, 75°, and 90° [vertical segmental baffle]) are used. The effect of baffle orientation on shell-and-tube heat exchanger performance is investigated. The flow domain is meshed by three-dimensional tetrahedral elements. The obtained result has a good agreement with the analytical method (i.e., the Bell-Delaware method) and experimental data in the literature. By comparing the pressure drop, heat transfer, and heat transfer versus pressure drop (Q/ P) at same flow rate, the shell-and-tube heat exchanger with 90° orientation performs better than other baffle orientation angles. The 90° orientation decreases pressure drop by 26%, 4.1%, 17.6%, 24.42%, and 14% more than the 15°, 30°, 45°, 60°, 75°, and 0° angles of orientation, respectively. This shows the 90° angle has better performance than other angles of baffle orientation. By reducing the pressure drop while maintaining the heat transfer rate, using this baffle orientation best reduces operating cost.

DOI: 10.22075/jhmtr.2017.1503.1100

1. Introduction

Heat exchangers are used often in various industries, such as the chemical industry, oil refining, power plant, food industry, etc. Various heat exchangers for industrial processes and systems have been designed. Among them, the shell-and-tube heat exchanger is the most common type [1–3]. The design of a new heat exchanger (HE) must address the sizing problem, construction type, flow arrangement, tube and shell material. This also includes the physical size, which has to meet the specified heat transfer and pressure drop. New HE designs must also meet the ratings of existing heat exchangers [4, 5]. More than 35–40% of heat exchangers are of the shell-and-tube type [6] Therefore, attention to this device is of great importance. In recent years, various types of baffles have been used in shell-and-tube heat exchanger. New designs have always aimed at keeping the pressure drop on the shell side reasonable despite the increase in the heat transfer rate. This reduces pumping and operational costs.

The rate of heat transfer in shell-and-tube heat exchangers is based on correlations between the Kern and Bell-Delaware method [7]. This method is used to calculate the pressure drop and heat transfer coefficient in shell-and-tube heat exchanger for fixed baffle cuts (25%), This method has some restrictions:

Corresponding Author : Department of Mechanical Engineering, University of Kashan, Kashan, Iran
Email : Mr.uosofvand@gmail.com

(1) it cannot adequately account for baffle-to-shell and tube-to-baffle leakage, and (2) this method is not applicable in laminar flow regions where the shell-side Reynolds number is less than 2,000 [8]. The Bell-Delaware method is more accurate than the Kern method. It can provide detailed results and predict and estimate the pressure drop and heat transfer coefficient with better accuracy. The method suggests the weaknesses in the shell-side design, but it cannot indicate the locations of the weaknesses [9]. The optimization of shell-and-tube heat exchangers requires a good understanding of the local and average shell-side heat transfer coefficients, which is complicated by shell diameter, baffle cut, baffle spacing, tube diameter, pitch, arrangement, and clearances or leakage paths. These leakages are one of the most important factors in reducing pressure drop and heat transfer coefficients on the shell side. If possible, the ability to show the field of flow and temperature allows for an easier computation of the position of weaknesses. Computational fluid dynamics can be useful to achieve this.

The most common baffle in shell-tube heat exchanger is the segmental baffle. The fluid flow is arranged in a zigzag pattern in this type of heat exchanger, resulting in a complicated leakage and bypass flow path [10]. For a given shell geometry, the ideal configuration depends on both the baffle cut and the baffle spacing. When these values are smaller than the ideal, the main stream passing the cut window is reflected by the next baffle and unwanted recirculation zones form (figure 1). When they are larger than ideal [11], the main stream follows a path near the next baffle and again recirculation zones form behind the baffle (figure 2). To understand the causes of the shell-side design weaknesses, the flow field inside the shell must be well understood. Ozden and Tari [11] numerically and experimentally investigated the flow characteristics of the shell-and-tube heat transfer at a laboratory scale. They showed the effect of baffle cut and baffle space on the heat transfer coefficient and pressure drop of shell-and-tube heat exchangers with different turbulence models. Raja and Ganne [12] used an inclined segmental baffle instead of the common segmental baffle and compared the pressure drop between them. A double shell-pass shell-and-tube heat exchanger with continuous helical baffles (STHXCH) has been invented to improve the shell-side performance of STHXCH. At the same flow area, a double shell-pass STHXCH was compared with a single shell-pass STHXCH and a conventional shell-and-tube heat exchanger with segmental baffles (STHXSG) [13]. The numerical results showed that the shell-side heat exchanger is slightly lower than that of STHXSG and 29–35% higher than that of single shell-pass STHXCH. The coefficients of the STHXCH are 12–17% and 14–25% higher than those of the STHXSG and single shell-pass STHXCH, respectively. Wang et al. proposed a combination of a multiple shell-pass shell and tube heat exchanger (CMSP-STHX) with continuous helical baffles in the outer shell pass to improve the heat transfer performance and simplify the manufacture process [14]. After comparing the CMSP-STHX with a conventional shell-tube heat exchanger with segmental baffles (SG-STHX) by means of computational fluid dynamic (CFD) method, they showed that under the same mass flow rate and the overall heat transfer rate (Q), the average overall pressure drop Δp of the CMSP-STHX was lower than that of the conventional SG-STHX by 13%. Under the same overall pressure drop (Δp) on the shell side, the overall heat transfer rate of the CMSP-STHX was nearly 5.6% higher than that of the SG-STHX, and the mass flow rate in the CMSP-STHX was about 6.6% higher than in the SG-STHX.

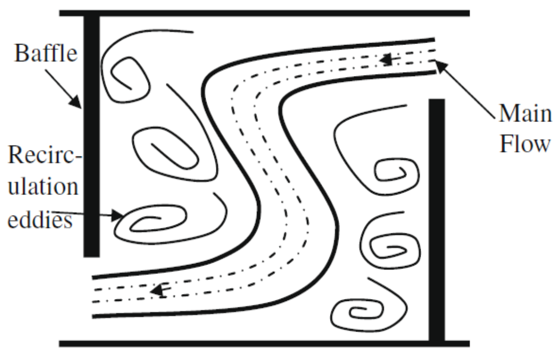

Fig. 1. Baffle distance smaller than ideal [11]

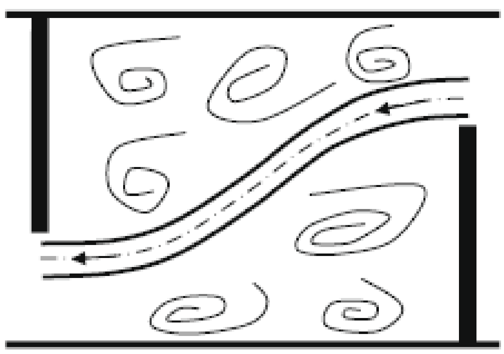

Fig. 2. Baffle distance bigger than ideal [11]

In the field of computational fluid dynamic, using alternative models is important in simulation in order to reduce computation time. Zhang et al. [15] simulated the shell-side flow and heat transfer for the whole heat exchanger by dividing the whole STHX into five cycles. The results showed that the relative difference between the 2nd cycle and 5th cycle was less than 2% for heat transfer and pressure drop. Because of the small differences between the result of one cycle and the other cycles, to reduce computing time, it is better to choose one cycle with a periodic condition. In other research based on selected cycles, an analysis of a heat exchanger with helical, middle-overlap baffles was carried out for different helix angles of 30°, 40°, and 50° [16]. The results showed the average heat transfer coefficient per unit of pressure drop was the largest with the 40° angle baffle.

Nemati et al. [17] showed the effect of baffle angle and baffle space on the performance of a heat exchanger with a helix baffle by means of CFD software. Zhang et al. [18] employed the CFD method to symmetrically study the thermodynamic and hydraulic performance of non-continuous helical baffles in helix angles ranging from 10° to 30°. Based on obtained results, helix baffles with 30° angles show the best performance over other angles. Jian et al. [19] proposed a new type of baffle, named the ladder-type fold baffle, to block the triangle leakage zones. The numerical results from this study showed that shell-side tangential velocity and radial velocity increased significantly in the improved heat exchanger In fact, the heat transfer coefficient in this new type increases by 82.8–86%.

In this paper, fluid flow is numerically simulated in a small (laboratory scale) shell-and-tube heat exchanger. The effect of baffle orientation on shell-and-tube heat exchanger performance is investigated. Baffles with the following angles were used: 0°, 30°, 45°, 60°, 75°, 90° (relative to the horizon). By comparing different parameters, such as the pressure drop, heat transfer, and the ratio of heat transfer to pressure drop, the angle that best increases the performance of shell-and-tube heat exchangers is identified.

2. Mathematical model

2.1 Geometry of shell-and-tube heat exchanger

In this study, a small shell-and-tube heat exchanger was selected. All design parameters of the shell-and-tube heat exchanger is based on Ozden and Tari's work [11]. Table 1 shows the design features of the shell-and-tube heat exchanger.

Table 1. Geometry of shell-and-tube heat exchanger [11]

Geometry	Size
Shell diameter	90 mm
Tube diameter	30 mm
Number of tubes	7
Heat exchanger length	600 mm
Shell side inner diameter	30 mm
Shell side outer diameter	30 mm
Baffle cut	36%
Central baffle spacing	86 mm

Figures 3(a), 3(b), and 3(c) show the shell-and-tube heat exchanger with different baffle orientation angles.

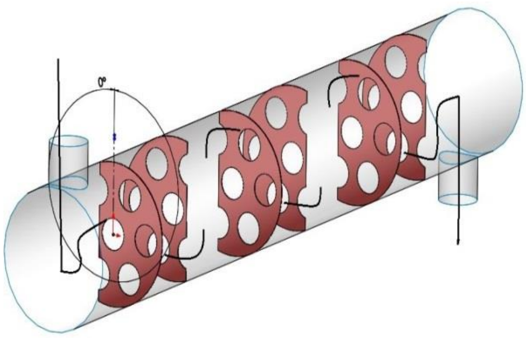

Fig. 3(a). Segmental baffle with a 0° angle of orientation

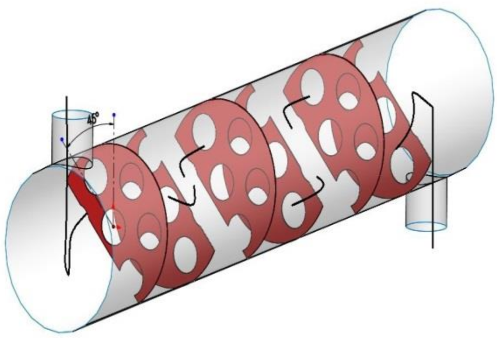

Fig. 3(b). Segmental baffle with a 15° angle of orientation

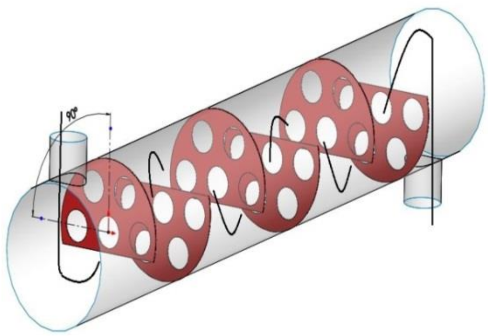

Fig. 3(c). Segmental baffle with a 90° angle of orientation

The other models (15°, 30°, 60°, 75°) are similar to the above pictures; for this reason, three of the models are shown.

2.2 Boundary conditions

To simplify the numerical simulation while still keeping the basic characteristics of the process, the following assumptions were made:

(1) The shell-side fluid has constant thermal properties.
(2) The fluid flow and heat transfer processes are turbulent and in a steady state.
(3) The leak flows between tube and baffle and between the baffle and the shell are neglected.
(4) The natural convection induced by the fluid density variation is neglected.
(5) The tube wall temperatures are kept at 450 K on the whole shell side.
(6) The heat exchanger is well-insulated; hence, the heat loss to the environment is totally neglected.

2.3 Numerical model

The commercial code Fluent was adopted to simulate the flow and heat transfer in the computational model. The governing equations along with the boundary conditions were iteratively solved by the finite volume method using the SIMPLE pressure-velocity coupling algorithm [20]. All the variables were treated with the second-order upwind scheme. The convergence criterions for residual monitoring were assumed to be 10^3 for the flow field and 10^6 for the energy equation, and some physically meaningful variables were also monitored, such as temperature and velocity [13]. The governing equations of continuity and momentum in the computational domain can be expressed as follows:

Continuity:

$$\nabla.(\rho\vec{V}) = 0\,. \tag{1}$$

X momentum:

$$\nabla.(\rho u\vec{V}) = -\frac{\partial p}{\partial x} + \frac{\partial \tau_{xx}}{\partial x} + \frac{\partial \tau_{yx}}{\partial y} + \frac{\partial \tau_{zx}}{\partial z}. \tag{2}$$

Y momentum:

$$\nabla.(\rho v\vec{V}) = -\frac{\partial p}{\partial y} + \frac{\partial \tau_{xy}}{\partial x} + \frac{\partial \tau_{yy}}{\partial y} + \frac{\partial \tau_{zy}}{\partial z} + \rho g. \tag{3}$$

Z momentum:

$$\nabla.(\rho w\vec{V}) = -\frac{\partial p}{\partial z} + \frac{\partial \tau_{xz}}{\partial x} + \frac{\partial \tau_{yz}}{\partial y} + \frac{\partial \tau_{zz}}{\partial z}. \tag{4}$$

Energy:

$$\nabla.(\rho e\vec{V}) = -\rho\nabla\vec{V} + \nabla.(k\nabla T) + q + \phi. \tag{5}$$

In the above equations *X*, *Y*, and *Z* inform the flow direction, and *U*, *V*, *W* represent the velocity in the direction of *X*, *Y*, and *Z*. Equation 5 is the dissipation function that can be calculated from

$$\phi = \mu[2\left[\left(\frac{\partial u}{\partial x}\right)^2 + \left(\frac{\partial v}{\partial y}\right)^2 + \left(\frac{\partial w}{\partial z}\right)^2\right] + \left(\frac{\partial u}{\partial y} + \frac{\partial v}{\partial x}\right)^2 + \left(\frac{\partial v}{\partial y} + \frac{\partial w}{\partial x}\right)^2 + \left(\frac{\partial v}{\partial z} + \frac{\partial w}{\partial y}\right)^2] + \lambda(\nabla.V)^2. \tag{6}$$

In Equation 6, λ and μ are the viscosity coefficient and dynamic viscosity, respectively.

2.3.1 Turbulence model

Since the flow is turbulent in this heat exchanger, the model of turbulence in the CFD simulation plays a vital role. In this study, to analyze the turbulent flow, the *k-ε* realizable was used. The standard *k-ε* model is a semi-empirical model based on model transport equations for the turbulence kinetic energy *k* and its dissipation rate ε . For a steady state, *k* and ε are obtained from the following transport equations:

In fact, the models for complex flows, such as rotary and curved flow, are more accurate than the standard model.

$$\frac{\partial}{\partial x_i}(\rho k u_i) = \frac{\partial}{\partial x_j}\left[\left(\mu + \frac{\mu_t}{\sigma_k}\right)\right]\frac{\partial k}{\partial x_j} + G_k + G_b - \rho_\varepsilon + s_k, \tag{7}$$

$$\frac{\partial}{\partial x_i}(\rho \varepsilon u_i) = \frac{\partial}{\partial x_i}\left[\left(\mu + \frac{\mu_t}{\sigma_z}\right)\frac{\partial t}{\partial x_j}\right] + C_{1z}\frac{\varepsilon}{k}(G_k + C_{3\varepsilon}G_b) - C_{2\varepsilon}\rho\frac{\varepsilon^2}{k} + S_\varepsilon. \tag{8}$$

The turbulent viscosity is defined by the following equation:

$$\mu_t = \rho C_\mu \frac{k^2}{\varepsilon}. \tag{9}$$

The model constants have the following values:

$$C_{1\varepsilon} = 1.44,\; C_{2\varepsilon} = 1.92, C_\mu = 0.09,\; G_k = 1, G_\varepsilon = 1.2\,. \tag{10}$$

2.3.2 Grid independency and validation

The flow domain for the shell side of a shell-and-tube heat exchanger was drawn with the SolidWorks software and then imported to the Gambit software. The obtained results for the shell-and-tube heat exchanger with a 90° baffle orientation were compared with the results from analytical methods (i.e., the Bell-Delaware method) and data from Ozden and Tari's research [11] in graphs for pressure drop (Figure 4) and temperature (Figure 5). This showed that the simulation was acceptable for the aforementioned shell-and-tube heat exchanger. The average differences between the current simulation with others in the literature are shown in Table 1.

The computational domain was created with tetrahedral cells using the Gambit software. In order to ensure the accuracy of the numerical results, a careful test for the mesh independence of the numerical solutions was conducted. In the test, three different mesh systems with 253,820, 627,960, and 1,938,709 elements were adopted for the calculation of the whole heat exchanger. According to the result in Figures 6 and 7, the temperature and pressure drop differences between the three models was less than 3%. Therefore, to save time and computational resources, the A model was selected for analysis.

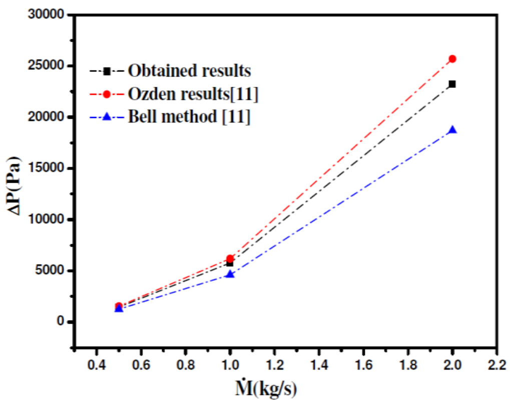

Fig. 4. Grid independency: pressure drop versus mass flow rate

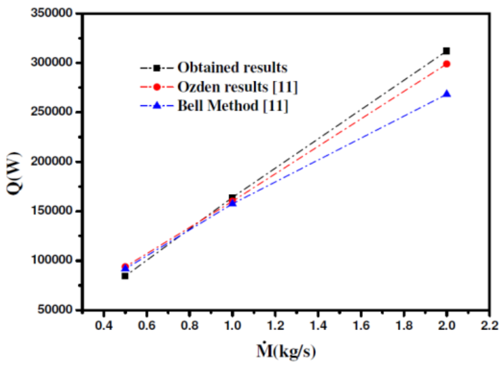

Fig. 5. Result validation: heat transfer vs mass flow

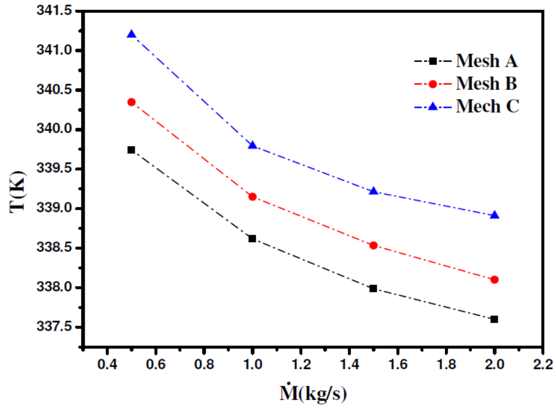

Fig. 6. Grid independency: temperature versus mass flow rate

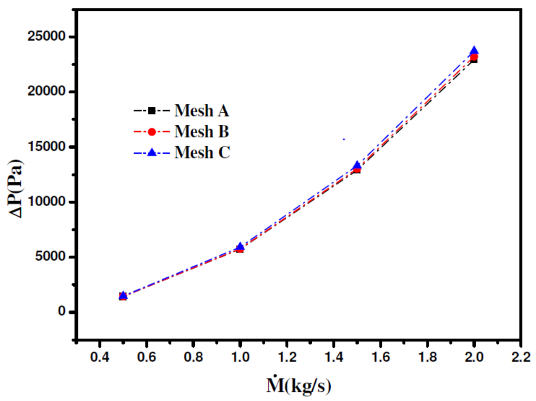

Fig. 7. Grid independency: pressure drop versus mass flow rate

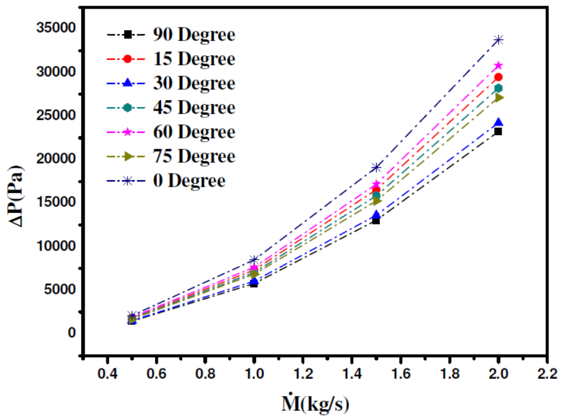

Fig. 8. Pressure gradient versus mass flow rate

Table 1: Results Validation

Average heat transfer differences between present work and the results of Ozden and Tari [11]	5.58%
Average pressure drop differences between present work with Ozden and Tari [11]	5.86%
Average heat transfer differences with the Bell-Delaware method [11]	9.4%
Average pressure drop differences between present work and Bell-Delaware method [11]	22.32%

3. Results and Discussion

3.1 Comparison of shell-side pressure drops with different baffles

Pressure drop is the most important parameter in the design of heat exchangers because if this parameter is low, the operating cost is low. Designers are always looking for a way to enhance heat transfer performance while maintaining a reasonable pressure drop. The angle of baffle positions and their arrangement play an important role in the shell-side heat transfer and fluid flow performance. In order to reduce the pressure drop of heat exchangers, one effective method is to increase the shell-side velocity of the heat exchanger by selecting the optimum angle of orientation in the design. The variations between shell-side pressure drop and mass flow rate are shown in Figure 8. It can be seen that the pressure drop increases with an increase of the shell-side mass flow rate, and its increase is more evident in the larger mass flow rates. At the same flow rate (0.5 kg/s to 2 kg/s), baffles with 0° angles of orientation (from vertical) with an average pressure of 15859.28 pa (N/M^2) have the maximum rate. In turn, baffles with 90° angles of orientation with a pressure of 10874.29 (N/M^2) have the minimum average rate. This angle reduces pressure drop by 26%, 4.1%, 17.6%, 24.42%, and 14% more than the 15°, 30°, 45°, 60°, 75°, 0° angles of orientation, respectively.

The local velocity vector distributions on the axial sections of the shell are shown in Figures 9 to 11. Whenever the angle between the flow direction and the axis of tube of STHXCH is smaller, the flow travels in the longitudinal direction. Therefore, it can reduce the pressure drop on the shell side and the vibration of the tube bundle. Based on velocity vectors, the longer the flow path, the greater the pressure drop, which can be seen by the fact that increasing the angle of orientation increases the pressure drop. Because the fluid must pass the two extra curved paths at the inlet and outlet of the heat exchanger at the 15°, 30°, 45°, 60°, 75° angles of rotation (Figures 1 and 2), these two curves cause the pressure drop to increase. Designers are always looking for a way to enhance heat transfer performance while maintaining a reasonable pressure drop. In fact, these two parameters in heat exchanger design are closely related.

3.2 Comparison of shell-side heat transfer

Figures 12 and 13 show a comparison of shell-side heat transfer within the range of the tested mass flow rates among the proposed baffle orientations of 0°, 15°, 30°, 45°, 60°, 75°, 90°. The results show that heat transfer increases with increases of the mass flow rate, and the highest heat transfer occurs in segmental baffles with 0° angles of orientation with an average heat transfer of 225.31 KW, and 90° baffle orientations have the minimum heat transfer rate with an average heat transfer of 200 kW. In fact, with an increase in the angle orientation, the heat transfer reduces at the same level. As a result, the longer the flow path, the greater the heat transfer. The contact time between the fluid and the tube is increased, thereby improving the heat transfer.

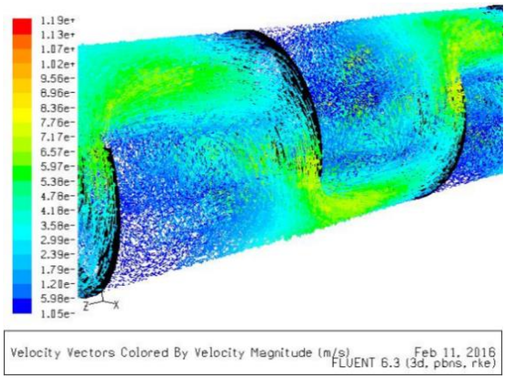

Fig. 9. Velocity vector for baffles with a 90° angle of orientation

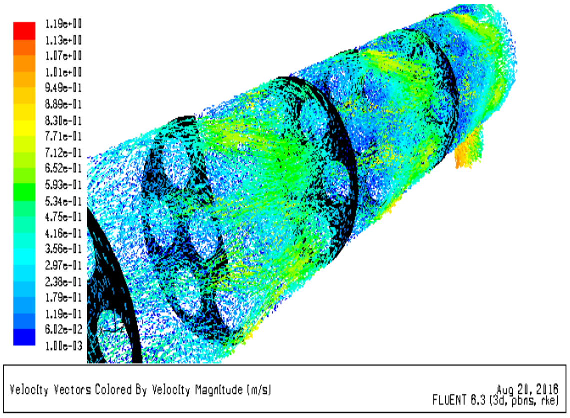

Fig. 10. Velocity vector for baffles with a 45° angle of orientation

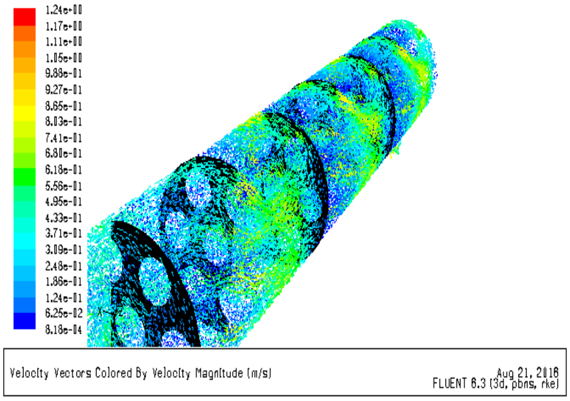

Fig. 11. Velocity vector for baffles with a 0° angle of orientation

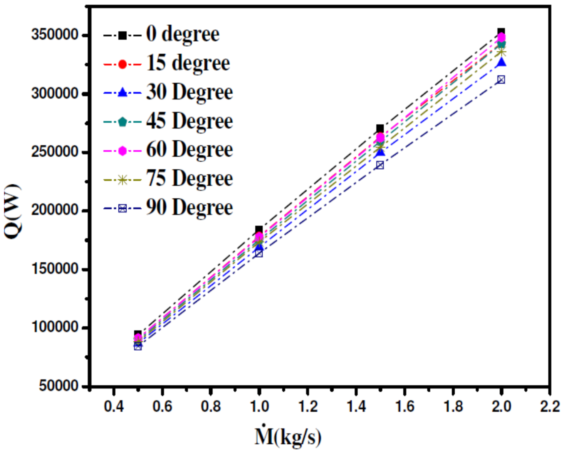

Fig. 12. Heat transfer versus mass flow rate

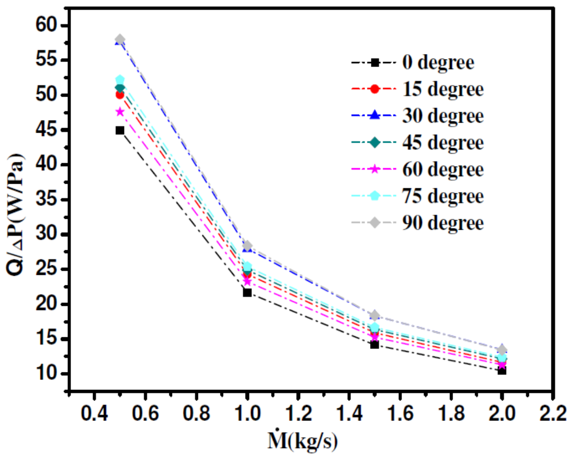

Fig. 13. Shell-side heat transfer per mass flow

4. Conclusion

Pressure drop and heat transfer are the two main factors in shell-and-tube heat exchangers. Based on the results among the 7 tested angles of orientation, a 90° baffle orientation showed the best performance among other orientations. Despite the loss of heat transference, this angle reduces pressure drop 26%, 4.1%, 17.6%, 24.42%, 14% more than the 15°, 30°، 45° ,60°,75° ,0° angles of orientation, respectively. The ratio of heat transfer per mass flow rate for baffles rotated 90° is better than other angles of rotation. This angle has minimum pressure drop compared to other models. Both heat transfer and pressure drop are critical qualities of heat exchanger performance. Comparing the heat transfer per pressure drop at the same flow rate in a 90° angle of orientation showed comprehensive performance (29.54 W/Pa), meaning that the amount of heat recovery at the same energy consumption to overcome friction is greater. Despite the loss of heat transfer compared to other angles, this model reduces pressure drop impressively. In fact, this reduction plays an important role in reducing pumping and operating cost. Therefore, the 90° angle of orientation represents a better choice over other angles of orientation.

Nomenclature

ρ	Density (kg.m^{-3})
P	Pressure (Pa)
C_p	Specific heat (J.kg^{-1}. K^{-1})
A_o	Heat exchange area based on the outer diameter of tube (mm^2)
h	Heat transfer coefficient (W.m^{-2}.K^{-1})
Q	Heat exchange quantity (W)
K	Thermal conductivity (W.m^{-1}.K^{-1})
μ	Dynamic viscosity of fluid (Pa.s^{-1})
D_s	Shell size diameter (mm)
G_k	Production of turbulence kinetic energy due to mean velocity gradients
σ_z `	Turbulent Prandtl numbers for ε
G_b	Generation of turbulence due to buoyancy
g	Gravitational acceleration (m/s^2)
C_1, C_2	Constants of transport equations
$C_{1\varepsilon}$	Constants of transport equations
$C_{2\varepsilon}$	Constants of transport equations
$x.y,z$	Direction of flow motion
Δp`	Shell-side pressure drop
$\dot{M}$	Mass flow rate (kg.s^{-1})
N	Number of tubes
ν	Kinematic viscosity of fluid, m^2 s^{-1}
L	Effective length of tube (mm)
Δt_m	Logarithmic mean temperature difference (K)
T	Temperature (K)
Re	Reynolds number
σ_v	Constant of transport equations
τ	Shear stress (N/m^2)
ϕ	Dissipation function
G_k	Production of turbulence kinetic energy due to mean velocity gradients
u, v, w	Velocity components (m/s)

References

[1]. Shah, R. K., & Secular, D. P. ‘‘Fundamentals of heat exchanger design’’, John Wiley &Soz, (2003).

[2].Kakaç S, Liu HT. Heat exchangers: Selection, rating and thermal design, CRC Press, (1997).

[3]. J.-F. Zhang, B. Li, W.-J. Huang, Y.-G. Lei, Y.-L. He, W.-Q. Tao, ‘‘Experimental Performance Comparison of Shell-Side Heat Transfer for Shell-and-Tube Heat Exchangers with Middle-Overlapped Helical Baffles and Segmental Baffles’’, Chemical Engineering Science, 64, 1643-53, (2009).

[4]. M. Thirumarimurugan, T. Kannadasan, E. Ramasamy, "Performance analysis of shell and tube heat exchanger using miscible system," American Journal of Applied Sciences, 5(5), 548-552, (2008).

[5]. K.S. Rao, ''Analysis of flow maldistribution in tubular heat exchangers by fluent," National Institute of Technology Rourkela, (2007).

[6]. B.I. Master, K.S. Chunangad, V. Pushpanathan, ''Fouling mitigation using helixchanger heat exchangers'', Engineering Conferences International, 366 (1Vol), (2003).

[7]. M. Salimpour, Heat transfer coefficients of shell and coiled tube heat exchangers, Experimental Thermal and Fluid Science, 33(2), 203-207, (2009)

[8]. Y.A. Kara, Ö. Güraras, ''A computer program for designing of shell-and-tube heat exchangers'', Applied Thermal Engineering, 24(13), 1797-1805, (2004).

[9]. U. Ur Rehman, ''Heat transfer optimization of shell-and-tube heat exchanger through CFD Studies'', Master thesis, Chalmers University of Technology, (2012).

[10]. J.-F. Zhang, Y.-L. He, W.-Q. Tao, ''A design and rating method for shell-and-tube heat exchangers with helical baffles'', Journal of Heat Transfer, 132(5), 051802-051802, (2010).

[11]. E. Ozden, I. Tari, ''Shell side CFD analysis of a small shell-and-tube heat exchanger,'' Energy Conversion and Management, 51(5), 1004-1014, 5//, (2010).

[12]. K.T.R. Raj, S. Ganne, ''Shell side numerical analysis of a shell and tube heat exchanger considering the effects of baffle inclination angle on fluid flow using CFD'', Thermal Science, 16(4), 1165-1174, (2012).

[13]. S. Ji, W.-j. Du, P. Wang et al., ''Numerical Investigation on Double Shell-Pass Shell-and-Tube Heat Exchanger with Continuous Helical Baffles'', Journal of Thermodynamics, 2011, 7, (2011).

[14]. Q. Wang, Q. Chen, G. Chen et al., ''Numerical investigation on combined multiple shell-pass shell-and-tube heat exchanger with continuous helical baffles,'' International Journal of Heat and Mass Transfer, 52(5), 1214-1222, (2009).

[15]. J.-F. Zhang, Y.-L. He, W.-Q. Tao, ''3D numerical simulation on shell-and-tube heat exchangers with middle-overlapped helical baffles and continuous baffles – Part I: Numerical model and results of whole heat exchanger with middle-overlapped helical baffles,'' International Journal of Heat and Mass Transfer, 52(23–24), 5371-5380, 11//, (2009).

[16]. J.-F. Zhang, Y.-L. He, and W.-Q. Tao, ''3D numerical simulation on shell-and-tube heat exchangers with middle-overlapped helical baffles and continuous baffles–Part II: Simulation results of periodic model and comparison between continuous and noncontinuous helical baffles,'' International Journal of Heat and Mass Transfer, 52(23), 5381-5389, (2009).

[17]. F. Nemati Taher, S. Zeyninejad Movassag, K. Razmi et al., ''Baffle space impact on the performance of helical baffle shell and tube heat exchangers'', Applied Thermal Engineering, 44, 143-149, 11//, (2012).

[18]. M. Zhang, F. Meng, Z. Geng, CFD simulation on shell-and-tube heat exchangers with small-angle helical baffles, Front. Chem. Sci. Eng., 9, 2, 183-193, 2015-07-14, (2015).

[19]. W. Jian, Y. Huizhu, S. Wang et al., "Numerical investigation on baffle configuration improvement of the heat exchanger with helical baffles," Energy Conversion and Management, 89, 438-448, (2015).

[20]. Fluent help 6.3.26 user's guide, FLUENT Inc, 2006, section 25. 4. 3.